Available online at www.sciencedirect.com
SCIENCE DIRECT
Catalysis Today 111 (2006) 94–102
CATALYSIS TODAY
www.elsevier.com/locate/cattod

Bridging the gap between liquid and vapor phase hydrocracking

J.W. Thybaut, C.S. Laxmi Narasimhan, G.B. Marin *

Laboratorium voor Petrochemische Techniek, Universiteit Gent, Krijgslaan 281, B-9000 Gent, Belgium

Available online 29 November 2005

Abstract

Research aimed at fundamental understanding of industrial reactions often leads to important differences, or so-called gaps, between laboratory and industrial conditions. Vapor and liquid phase hydrocracking of parapur, a mixture of linear alkanes in the range from C_9 to C_{14}, has been performed on a Pt/H-USY zeolite at temperatures between 503 and 533 K, total pressures between 1 and 7.7 MPa and molar inlet hydrogen to hydrocarbon ratios from 3 to 300. At these conditions ideal hydrocracking occurs, except for the heaviest components at the highest temperatures, lowest pressures and highest molar inlet hydrogen to hydrocarbon ratios. The individual component product distributions obtained at vapor and liquid phase conditions were identical to those reported in the literature for pure *n*-alkane hydrocracking. A preferential conversion of the heavier hydrocarbons in the mixture was observed for vapor phase parapur hydrocracking. At liquid phase conditions this preferential conversion of heavier hydrocarbons is still observed, but much less pronounced.

A single kinetic model accounting for all these features allows to adequately describe both vapor and liquid phase parapur hydrocracking. It suffices to account explicitly for (i) the non-ideality of the fluid phase, (ii) the destabilization of the physisorbed phase in the catalyst micropores and (iii) the increased strength of the acid sites at the liquid phase conditions. The last two effects are quantified by so-called physisorption and protonation excess.
© 2005 Elsevier B.V. All rights reserved.

Keywords: Liquid and vapor phases; Gap; Hydrocracking; Microkinetics; Aggregation state; Single event; Physisorption

1. Introduction

Refinery product streams consist of thousands of components [1–3]. In refinery conversion processes all these components are subject to an even higher number of elementary steps. However, all elementary steps can be classified in a relatively low number of reaction families such as (de)-protonation, alkyl-shift, β-scission, hydride transfer, alkylation, etc. [4,5]. As a result, laboratory research can focus on the behavior of model components that are susceptible to elementary steps belonging to the same reaction families. The use of model components provides several advantages:

1. The more limited number of components involved in the reaction mixture renders the effluent analysis easier.
2. Lower carbon number molecules can be used as model components and, hence, typical problems with heavier molecules such as condensation, viscosity, etc. can be avoided.

On the other hand, the use of model components may lead to a 'gap' between the laboratory and industrial conditions [6,7]. This 'gap' can be limited to temperature and pressure differences, but it can be as important as aggregation state differences, e.g. hydrocracking of industrial feedstocks is performed at three-phase conditions [2], i.e. gas–liquid–solid, while laboratory model component research is frequently performed at vapor phase conditions [8–10]. Working at vapor phase conditions is easier than at liquid phase conditions from the analytical and set-up construction point of view. In addition it also allows to observe the chemical phenomena involved undisguised by vapor–liquid phase transfer and/or not having to account for additional equilibrium phenomena. Hence, vapor phase investigation of reactions such as hydrocracking will lead to more unambiguous kinetic information. To enable reliable scale-up to industrial conditions, the 'gap' between vapor and liquid phase conditions has to be bridged. Liquid phase experimentation is also being performed at laboratory scale to assess aggregation state-related effects on the kinetics obtained at vapor phase conditions [11,12].

Hydrocracking is a bifunctional process [13–15]. Saturated reactants are dehydrogenated at metal sites yielding unsaturated

* Corresponding author. Tel.: +32 9 2644516; fax: +32 9 2644999.
E-mail address: Guy.Marin@UGent.be (G.B. Marin).

0920-5861/$ – see front matter © 2005 Elsevier B.V. All rights reserved.
doi:10.1016/j.cattod.2005.10.001

Nomenclature

AS	alkyl-shift
b	model parameter vector containing the estimated parameter values
C	concentration [mol kg_{cat}^{-1}]
C_t	total concentration of acid sites [mol kg_{cat}^{-1}]
c^E	scaling factor between the excess free enthalpy for physisorption and the liquid phase fugacity coefficient [kJ mol^{-1}]
F	molar flow rate [mol s^{-1}]
f	fugacity [MPa]
G	free enthalpy
g	lump
H	Henry coefficient [mol kg_{cat}^{-1} MPa^{-1}]
H	enthalpy [J mol^{-1}]
h	lump
K_{deh}	equilibrium coefficient for dehydrogenation [MPa]
$K_{isom}(O_{i,j}; O_r)$	equilibrium coefficient for isomerization between alkene j and the reference alkene
K_L	Langmuir physisorption coefficient [MPa^{-1}]
$K_{prot}(O_{i,j}; m)$	equilibrium coefficient for protonation of alkene j with formation of a carbenium ion of type m [kg_{cat} mol^{-1}]
k(m; n)	rate coefficient of a reaction converting a carbenium ion of type m into another carbenium ion of type n [s^{-1}]
LC	lumping coefficient [MPa]
m	carbenium ion type (secondary or tertiary)
n	carbenium ion type (secondary or tertiary)
nob	number of observations
nresp	number of responses
$O_{i,j}$	alkene j stemming from alkane i
P_i	alkane i
PCP	protonated cyclo-propane
p	partial pressure [MPa]
$R_{i,j}$	net production rate of component j in experiment i [mol $(kg\ s)^{-1}$]
$r_{m,n}$	rate of a reaction converting a carbenium ion of type m into another carbenium ion of type n [mol $(kg\ s)^{-1}$]
s	secondary
SSQ	sum of squares [$mol^2\ s^{-2}$]
t	tertiary
V_m	molar volume [m^3 mol^{-1}]
W_i	catalyst weight in experiment i [kg]
X	conversion
y	mole fraction

Greek symbols

β	β-scission
β	model parameter vector containing the real parameter values
Δ	difference
ϕ	fugacity coefficient [−]
σ	symmetry number
$\sigma^{-1}_{j,k}$	element on the jth row and kth column of the inverse of the variance covariance matrix of the experimental errors

Superscripts

^	model-calculated value
∼	single-event
0	standard
E	excess
G	gas/vapor
L	liquid

Subscripts

≠	transition state
0	inlet
deh	dehydrogenation
i	component number
isom	isomerization
lump	relumped
phys	physisorption, physical
prot	protonation
ref	reference
sat	saturation

species. These unsaturated species move to the acid sites where they are protonated yielding carbenium ions. These carbenium ions are susceptible to the actual isomerization and cracking reactions. The product carbenium ions desorb from the acid site via deprotonation. The resulting unsaturated species are hydrogenated at the metal sites yielding the observable saturated isomerized and cracked products. Prior to these chemical elementary steps in hydrocracking a physisorption step occurs [16,17]. At vapor phase conditions this physisorption acts as a condensation and leads to an enrichment of the reactants on the catalyst. On the one hand, the metal function on hydrocracking catalysts is serving as a source of unsaturated species. On the other hand it also acts as a sink removing an excess of unsaturated species and, hence, avoiding catalyst deactivation. Typical laboratory experiments focus on the acid-catalyzed steps in hydrocracking and, hence, operating conditions are selected at which the metal-catalyzed (de)-hydrogenations are in quasi-equilibrium, i.e. so-called ideal hydrocracking conditions. The occurrence of secondary cracking is minimal at these conditions.

The present work focuses on the 'gap' in the aggregation state between vapor and liquid phase hydrocracking. Mixture effects are addressed simultaneously by the use of an *n*-alkane mixture rather than a pure model component. Experiments have been performed at vapor and liquid phase conditions using the same feedstock. The kinetic modelling of the resulting data allowed the assessment of aggregation state effects on the kinetics.

2. Procedures

2.1. Hydrocracking experiments

Hydrocracking experiments have been performed using parapur as a feedstock at the operating conditions mentioned in

Table 1
Operating conditions and space times used in the parapur hydrocracking experiments

	Gas phase	Liquid phase
Temperature (K)	503–523	513–533
Total pressure (MPa)	1–3	6–7.7
Molar inlet H_2/HC ratio (−)	50–300	3–8
Space time (kg s mol^{-1})	180–1100	250–650

Table 1. Parapur is a commercially available mixture of linear alkanes with carbon numbers ranging from 9 to 14. The main constituents are decane, 10 mol%, undecane, 26 wt.%, dodecane, 44 wt.%, and tridecane, 19 wt.%.

The catalyst used was MC-389. It contains 65 wt.% LZ-Y20 [18] as H-USY-zeolitic component and 35 wt.% alumina binder. The zeolite has a framework silicon to aluminum ratio of 29. The total acid site concentration has been determined using quantitative ^{27}Al MAS-NMR and amounted to 0.237 mol kg^{-1}. 1. Platinum (0.64 wt.%) was deposited on the catalyst as metallic function with a dispersion close to 1. The catalyst pellet size ranged between 0.5 and 0.8 mm. The absence of concentration and temperature gradients has been verified, e.g. the maximum Weisz moduli obtained were below 10^{-2}.

The vapor phase experiments have been performed in a Berty reactor [19]. Liquid parapur is fed using an HPLC-pump and is vaporized and mixed with the gaseous reactants in an evaporator/preheater. A stirrer ensures the complete mixing inside the Berty reactor to ensure the CSTR behavior of the reactor. The catalyst bed is located centrally in the reactor. The stirrer is located at the bottom of the reactor and establishes an upflow between the catalyst bed and the reactor wall and a downflow through the catalyst bed. A schematic drawing of this set-up has been reported by Steijns et al. [20]. The quality of the hydrogen used (99.99%, L'Air Liquide, $H_2O + O_2$ content <10 ppm) made further purification of the hydrogen feed unnecessary. The hydrocarbon feed flow rate was verified by monitoring the mass of the feed reservoir. Methane was used as the internal standard. The reactor effluent is sampled on-line and sent to an HP series II 5890 instrument with a 50-m (i.d.: 0.25 mm) RSL-150 column with a 0.25-ím poly(dimethylsiloxane) film and an FID detector. Cryogenic cooling allowed for separation of the lighter compounds.

A Robinson-Mahoney reactor was used for the liquid phase experiments [21]. This reactor is also equipped with a stirrer to ensure the complete mixing of the reaction mixture. The catalyst is contained in a concentric, cylindrical basket. Liquid and gas enter the reactor via the bottom and leave it through an overflow located at the top of the reactor. A radial flow pattern is induced by the stirrer from the centre to the reactor wall through the catalyst basket. Recirculation occurs above and below the catalyst basket. The liquid phase is the continuous phase in the reactor containing dispersed gas bubbles. The reactor effluent is separated in a gas and a liquid flow using a cyclone followed by a demister. The gas effluent can be analyzed on-line and is evacuated continuously while the liquid effluent is discharged periodically via an automated procedure and is analyzed off-line. More details about this experimental set-up, including a schematic drawing, can be found in the work of Arroyo et al. [11].

2.2. Outlet flow rates and conversions

The effluent composition from the vapor phase set-up is determined only in terms of hydrocarbons. The mass and carbon balance over the reactor is monitored by adding an internal standard, e.g. methane, to the effluent between the reactor outlet and the on-line sampling valve. Based on the methane flow rate added to the effluent and its FID analysis the corresponding molar flow rates of the components in the effluent are obtained. Minor amounts of methane and ethane can, however, be produced during reaction due to hydrogenolysis. The non-occurrence of hydrogenolysis is verified via experiments without internal standard.

The liquid phase reactor effluent is splitted into three outlet streams, i.e. (1) the gas-phase effluent, denoted as F^{G}, (2) the flashed gas effluent, F^{LG}, and (3) the flashed liquid effluent, F^{LL}. The volumetric flow rates of the flashed gas and flashed liquid effluent are measured. The corresponding molar flow rates are obtained by application of the ideal gas law and by calculating the liquid molar volume using the Hankinson–Brobst–Thomson method 22. The gas effluent flow rates are obtained using an internal standard, similar to the vapor phase experiments. The total outlet flow rate of component i is obtained by summation:

$$F_i = F_i^{G} + F_i^{LG} + F_i^{LL} \tag{1}$$

Individual component conversions are defined as

$$X_i = \frac{F_{i,0} - F_i}{F_{i,0}} \tag{2}$$

The mixture conversion is calculated from the individual conversions by weighing them using the feedstock mole fractions, $y_{i,0}$:

$$X_{\text{mixture}} = \sum_i y_{i,0} \frac{\mathrm{F}_{i,0} - F_i}{F_{i,0}} \tag{3}$$

2.3. Parameter estimation

Parameter estimations were performed using the Rosenbrock method [23] for the initial minimization for the objective function, i.e. when the current parameter values are still remote from the final optimal values. For the final optimization a Marquardt algorithm [24] was used. A self-written algorithm was used for the Rosenbrock method, while for the Marquardt algorithm the 'ordinary least squares' (OLS) option of the ODRPACK-package version 2.01 [25] was used. Some additional source code was added to ODRPACK in order to retrieve additional statistical information.

The objective function used in the above methods is the weighed sum of the squared differences, SSQ(b) between the observed and the calculated outlet flow rates using a full variance–covariance matrix of the experimental errors on the responses. The objective function was minimized by

adjusting the model parameter vector $\boldsymbol{b}$, which is expected to approach the real parameter vector $\boldsymbol{\beta}$ when the optimum is reached:

$$\mathrm{SSQ(b)} = \sum_{i=1}^{\mathrm{nob}} \sum_{j=1}^{\mathrm{nresp}} \sum_{k=1}^{\mathrm{nresp}} \sigma_{j,k}^{-1} (F_{j,i} - \hat{F}_{j,i})(F_{k,i} - \hat{F}_{k,i}) \xrightarrow{\boldsymbol{b}} \min \quad (4)$$

$\sigma_{j,k}^{-1}$ are the elements of the inverse of the variance–covariance matrix of the experimental errors. This matrix is calculated from replicate experiments or, when no replicate experiments are available, it can be estimated from the observed and calculated outlet flow rates.

The outlet flow rates were calculated according to the model equations presented in the following two sections.

2.4. Reactor model

Both the Berty and the Robinson-Mahoney reactor are CSTR-type reactors. As a result, reactor mass balances for the individual components j in experiment i lead to a set of algebraic equations in both cases:

$$F_{i,j} - F_{0,i,j} - R_{i,j} W_i = 0 \quad (5)$$

W_i being the catalyst mass used in experiment i and $R_{i,j}$ being the net rate of formation of component j at the reaction conditions of experiment i.

In the Berty reactor all reactants and products are in the vapor phase. As a result, the partial pressures of the components in the reactant mixture in contact with the catalyst can be directly calculated. In the Robinson-Mahoney reactor, the components are distributed over the vapor and liquid phase. At typical operating conditions, the catalyst in a Robinson-Mahoney reactor is completely wetted and, hence, liquid phase concentrations have to be obtained from the global reactant mixture composition for reaction rate calculation. Because the experiments are being performed at intrinsic kinetic conditions and, hence, no transport limitations are occurring between the vapor and the liquid phase, the liquid phase concentrations can be obtained from an equilibrium calculation 22.

2.5. The single-event microkinetic model

Within the reaction families considered in hydrocracking, the rate coefficients are assumed to depend on the type, n or m, cfr. Eq. (6), of the carbenium ions involved as reactant and/or product, secondary or tertiary. The only other structural feature of the reactive moiety which needs to be accounted for is the symmetry number. The ratio of the symmetry number of the reactant, e.g. $\sigma_{\mathrm{O}_{i,j}}$, to that of the transition state, e.g. $\sigma_{\neq ikqr}$, equals the number of so-called single-events 26.

Reaction rates for the acid-catalyzed elementary steps in hydrocracking can be expressed as follows when the metal-catalyzed (de)-hydrogenation reactions are in quasi equilibrium:

$$r_{\mathrm{m}_{i,k};n_{q,r}}^{\mathrm{AS/PCP}/\beta} = \frac{C_{\mathrm{t}} \sigma_{\mathrm{O}_{i,j}} / \sigma_{\neq ikqr} \tilde{k}^{\mathrm{AS/PCP}/\beta}(\mathrm{m;n}) \tilde{K}_{\mathrm{prot,O_{ref};m}} \tilde{K}_{\mathrm{isom,O_{i,j};O_{ref}}} K_{\mathrm{deh,P}_i;\mathrm{O}_{i,j}} C_{\mathrm{sat,P}_i} K_{\mathrm{L,P}_i} p_{\mathrm{P}_i} / p_{\mathrm{H_2}}}{1 + \sum_{j=1}^{n} K_{\mathrm{L,P}_j} p_{\mathrm{P}_j}} \quad (6)$$

The coefficients in Eq. (6) have their usual meaning and are explained in Nomenclature. It was assumed in the derivation of this rate that the carbenium ion concentrations were negligible. At lower total pressures this assumption is not always holding. In such a situation it suffices to replace the denominator in this equation by an expression accounting for the carbenium ion concentrations [27]. For more-detailed information on the single-event model, the reader is referred to previous publications by our group [4,10,26–28].

The net rate of formation of an alkane i is expressed as the sum of all rates of elementary steps in which the carbenium ions k, corresponding with alkane i are produced minus the rates of all elementary steps in which those carbenium ions k are consumed. It is obvious that, especially for heavier hydrocarbons, these summations can become very time consuming. Also, the present analytical techniques do not allow a specification of feedstocks in full detail. The relumped single-event microkinetic model is the answer to the above remarks. The individual components are lumped and reaction rates are calculated between these lumps. However, the calculated reaction rates fully account for all possible elementary steps between the lumps. The only assumption required in the relumped single-event microkinetic model is related to the specification of the internal composition of the lumps. The lumps are defined in such a way that thermodynamic equilibrium can be assumed in hydrocracking on Pt/H-USY-zeolite. In the relumped model for alkane hydrocracking four lumps are considered per carbon number, i.e. *n*-alkane, mono-, di-, and tri-branched alkanes.

The reaction rate between lumps g and h, $r^{\mathrm{PCP}}(\mathrm{g;\ h})$ corresponds to the summation of the reaction rates of all the elementary steps occurring between species of lumps g and h [4,10,26]. For, e.g. the PCP-reactions between two isomer lumps g and h this results in:

$$r^{\mathrm{PCP}}(\mathrm{g;h}) = \frac{k_{\mathrm{lump}}^{\mathrm{PCP}}(\mathrm{g;h}) H_{\mathrm{g}} p_{\mathrm{g}} / p_{\mathrm{H_2}}}{1 + \sum_{\mathrm{f}} K_{\mathrm{L,f}} p_{\mathrm{f}}} \quad (7)$$

where the lumped rate coefficient $k_{\mathrm{lump}}^{\mathrm{PCP}}(\mathrm{g;h})$ is a function of the fundamental rate coefficients. Hence, the fundamental charac-

ter of the model is preserved. The lumped rate coefficient also depends on the so-called lumping coefficients, LC:

$$k_{\text{lump}}^{\text{PCP}}(\text{g};\text{h}) = [LC_{\text{s;s}}^{\text{PCP}}(\text{g};\text{h})\tilde{K}_{\text{prot}}(\text{s})\tilde{k}^{\text{PCP}}(\text{s};\text{s}) + \text{LC}_{\text{s;t}}^{\text{PCP}}(\text{g};\text{h})\tilde{K}_{\text{prot}}(\text{s})\tilde{k}^{\text{PCP}}(\text{s};\text{t}) + \text{LC}_{\text{t;s}}^{\text{PCP}}(\text{g};\text{h})\tilde{K}_{\text{prot}}(\text{t})\tilde{k}^{\text{PCP}}(\text{t};\text{s}) + LC_{\text{t;t}}^{\text{PCP}}(\text{g};\text{h})\tilde{K}_{\text{prot}}(\text{t})\tilde{k}^{\text{PCP}}(\text{t};\text{t})]C_{\text{t}} \quad (8)$$

The latter are independent of the single-event rate coefficients as is seen from Eq. (9):

$$\text{LC}_{\text{m;n}}^{\text{PCP}}(\text{g};\text{h}) = \sum_{i\in\text{g}}\sum_{k\in\text{g}}\sum_{q\in\text{h}}\sum_{r\in\text{h}}\frac{\sigma_{\text{O}_{i,j}}}{\sigma^{\neq}_{ikqr}}K_{\text{iso}}(\text{O}_{i,j};\text{O}_{\text{ref}})K_{\text{deh}}(\text{P}_i;\text{O}_{i,j})y_{i,\text{g}} \quad (9)$$

Each term of the right-hand side of Eq. (9) consists of values that are known via the reaction network or that can be calculated based on thermodynamic data. The specification of the mole fractions $y_{i,\text{g}}$ of the components i in lump g, is the only concession that has to be made to preserve the fundamental character of the relumped model. As mentioned above, a judicious definition of the lumps allows to assume that equilibrium is established within the lumps [4,10,26].

3. Parapur hydrocracking

The discussion of the experimental results is focused on the behavior of the main parapur constituents, i.e. decane, undecane, dodecane and tridecane. The decane conversion can be somewhat underestimated because it can be formed out of tridecane isomers through slow (s; s) β-scission. However, this is not interfering with the main conclusions drawn from the interpretation of the experimental results.

3.1. Vapor phase hydrocracking

The parapur conversion increases with the temperature and the space time, vide Fig. 1a and b [30]. The conversion increases with decreasing total pressure and inlet molar hydrogen to hydrocarbon ratio. These effects can be rationalized from the rate equation applicable at ideal hydrocracking conditions [8,16,29], vide Eq. (6). In particular the parapur conversion increase upon a total pressure decrease is related to the alkane/alkene (de)-hydrogenation equilibrium which is more to the side of the alkenes at lower total pressures [29].

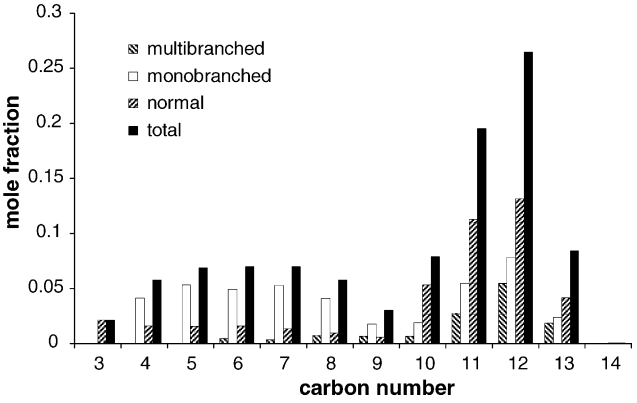

Fig. 2. Parapur hydrocracking molar effluent composition at 523 K, 2 MPa and inlet molar H_2 to hydrocarbon ratio 200 with a space time of 350 kg s mol^{-1} in terms of carbon number and branching degree.

Fig. 2 shows the effluent composition in terms of carbon number and branching degree at 523 K, 2 MPa and a molar inlet H_2 to hydrocarbon ration of 200 with a space time of 350 kg s mol^{-1}. At these conditions a total conversion of 57% is obtained, from which 38% to isomers and 19% to cracked products. The isomers are mainly monobranched. Multibranched isomer formation occurs consecutively to monobranched isomer formation. Moreover, multibranched isomers undergo faster cracking reactions. The cracked product distribution, i.e. from C_3 to C_9, is practically symmetric around C_6. Such symmetry is typical for pure component hydrocracking without secondary cracking. The fact that this symmetry is also observed in parapur hydrocracking indicates that the cracked product distribution at the investigated conditions is governed by the cracking of the *n*-dodecane in the parapur and that no secondary cracking occurs.

The total parapur conversion always behaved according to the observations described above.

The individual component conversion versus the total parapur conversion in vapor phase hydrocracking is shown

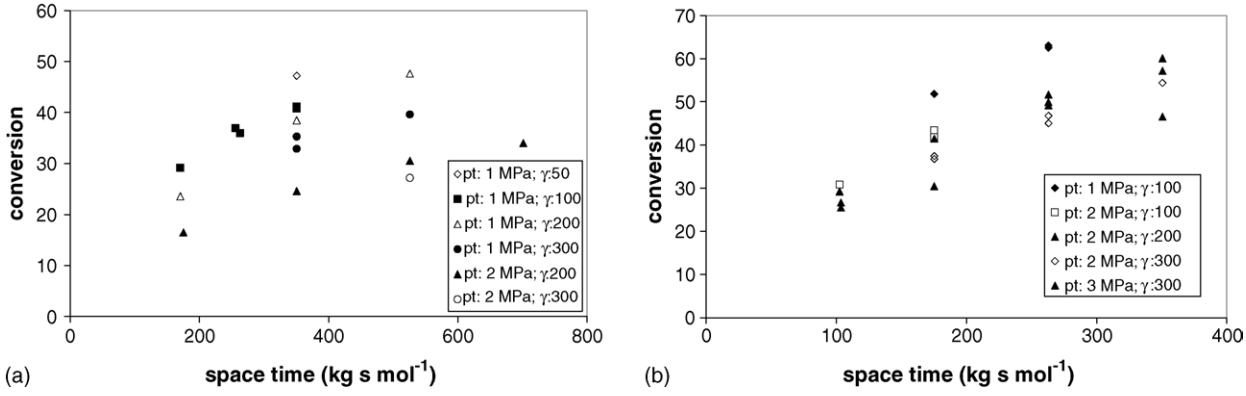

Fig. 1. Parapur conversion as a function of space time: effect of total pressure and inlet molar hydrogen to hydrocarbon ratio at (a) 503 K and (b) 523 K [30].

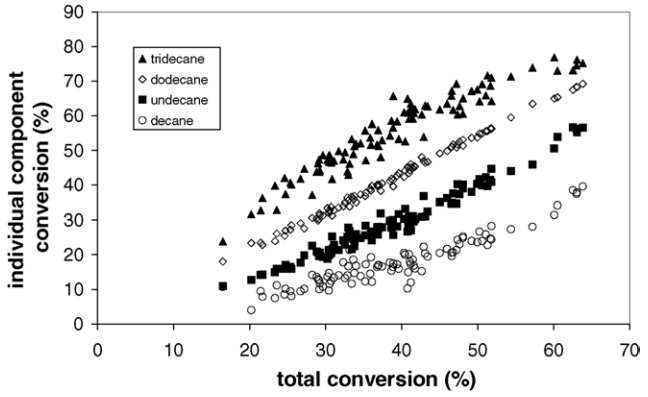

Fig. 3. Individual component conversion versus total parapur conversion in vapor phase hydrocracking at 503–523 K, 1–3 MPa and molar inlet hydrogen to hydrocarbon ratios between 50 and 300 [30].

in Fig. 3 [30]. Individual component conversions increase with the carbon number. The preferential conversion of heavier components is related to their preferential physisorption as well as to their higher intrinsic reactivity. Henry coefficients increase exponentially with carbon number explaining the preferential physisorption. The higher intrinsic reactivity is explained by the increasing number of possible PCP-reactions and β-scissions with carbon number.

The individual component behavior in parapur hydrocracking is not always occurring according to ideal hydrocracking. Especially for the higher carbon number alkanes deviations from ideal hydrocracking behavior are observed at higher temperatures, lower total pressures and higher molar inlet hydrogen to hydrocarbon ratios. Deviations from ideal hydrocracking are evident from the total pressure effect on the (individual) component conversion but are also reflected by the lower isomer conversions at such conditions [8,29]. The experimental data can be grouped according to the deviation from ideal tridecane hydrocracking [8,29]. The higher the group number, the stronger the deviation from ideal hydrocracking. Table 2 lists the ratio of the actual isomerization conversion to the isomerization conversion obtained at ideal

Table 2
Ratio of actual isomerization conversion to isomerization conversion at ideal hydrocracking for the individual components in parapur [30]

	Group 0	Group 1	Group 2
Decane	1	1	1
Undecane	1	1	0.94
Dodecane	1	0.86	0.8
Tridecane	1	0.76	0.52

hydrocracking for the main components in parapur [30]. Within a group the lowest values are obtained for the heaviest components, indicating the more pronounced non-ideal hydrocracking behavior of these heavier components.

The assessment of the isomerization conversion and isomer distribution for the individual components leads to identical conclusions, irrespective of the selected component. Because a wealth of literature data is available, dodecane [15,16,31–33] is chosen for this assessment. The maximum isomerization conversion of dodecane in parapur amounted to 40% at a total dodecane conversion of 50%. Similar values were obtained using pure dodecane as feedstock [15,16,32], indicating that the other components in the mixture are not chemically interacting with dodecane. The only effects observed between the components in the mixture are related to competitive physisorption. The distribution of the dodecane methyl-branched isomers is shown at low and high conversion, vide Tables 3a and 3b [30]. At low conversion, Table 3a, the methyl-branched isomer distribution is kinetically controlled. Because methyl branching rates are independent of the branching position, the number of possible reaction pathways between the methyl-branched isomer and dodecane is reflected in the methyl-branched isomer distribution at low conversion. Twice as many $3MeC_{11}$ is observed as $2MeC_{11}$, which corresponds to twice as many reaction pathways between $3MeC_{11}$ and dodecane as between $2MeC_{11}$ and dodecane. The same reasoning can be extended to the other methyl-branched isomers. At higher conversions the methyl-branched isomer distribution tends to the equilibrium distribution. The inter-

Table 3a
Dodecane methyl-branched isomer distribution: comparison between reported distributions at low conversion ($0\% < X < 10\%$)

	This work	Steijns and Froment [16]	Weitkamp [32]	Weitkamp and Hedden [15]	Martens and Jacobs [33]
$2MeC_{11}$	14	13	10.8	13.6	13.1
$3MeC_{11}$	24	25	20.4	24.3	24.9
$4MeC_{11}$	26	24	25.4	23	23.9
$5 + 6MeC_{11}$	36	38	43.4	39.1	38.1

Table 3b
Dodecane methyl-branched isomer distribution: comparison between reported distributions at high conversion ($X > 50\%$)

	Equilibrium[a]	This work	Steijns and Froment [16]	Weitkamp [32]	Weitkamp and Hedden [15]	Schulz and Weitkamp [31]
$2MeC_{11}$	24.7	21	20.5	20.8	19.7	19.7
$3MeC_{11}$	26.3	24	23.5	22.9	23.8	23.9
$4MeC_{11}$	19.7	21	20	19.1	19	18.8
$5 + 6MeC_{11}$	29.3	32	36	37.2	37.5	37.7

conversion between methyl-branched isomers is fast compared to the production and consumption of these isomers through PCP branching reactions. The agreement between the dodecane isomer distributions obtained in an *n*-alkane mixture in this work and with pure dodecane in the literature indicates that no mixture effects occur on the dodecane reaction network. As already evident from the total isomerization conversion, the only effects observed when using a mixture as feedstock are competitive physisorption effects.

3.2. Liquid phase hydrocracking

At liquid phase conditions, the parapur hydrocracking conversion increases with temperature and space time, it decreases with the total pressure and is not affected by the molar inlet hydrogen to hydrocarbon ratio. While the first three effects correspond to those observed at vapor phase conditions, the latter is exclusively observed at liquid phase conditions. It is related to the full wetting of the catalyst and the fact that, at a given temperature and hydrogen partial pressure, the hydrogen solubility in the liquid phase does not depend on the hydrogen inlet flow rate. As a result, the reaction rate is not affected by the molar inlet hydrogen to hydrocarbon ratio.

Product distributions appeared to be independent of the aggregation state of the reaction mixture. At liquid phase conditions no deviations from ideal hydrocracking have been observed. Isomerization conversions were corresponding to those obtained at ideal hydrocracking in the entire range of operating conditions because of the high pressures and low molar inlet hydrogen to hydrocarbon ratios used. The similarity between product distributions obtained at vapor and liquid phase conditions indicates that mixture effects at liquid phase conditions are also limited to competitive physisorption.

The main difference between vapor and liquid phase hydrocracking is observed when comparing the individual component conversions to the total parapur conversion, vide Fig. 4 [30]. The individual conversions obtained at liquid phase conditions are closer to each other than at vapor phase conditions [34,35], vide Table 4. This is related to differences in physisorption behavior depending on the aggregation state [36]. At liquid phase conditions saturation of the catalyst pores occurs and physisorption properties are becoming carbon number independent. At vapor phase conditions, physisorption is governed by the Henry coefficients which exhibit an exponential dependence on carbon number. As a result only the higher intrinsic reactivity of the components remains to cause a preferential conversion of the heavier components at liquid phase conditions, cfr. Section 3.1. The introduction of the aggregation state-dependent physisorption behavior into the single-event microkinetic model is the subject of the following section.

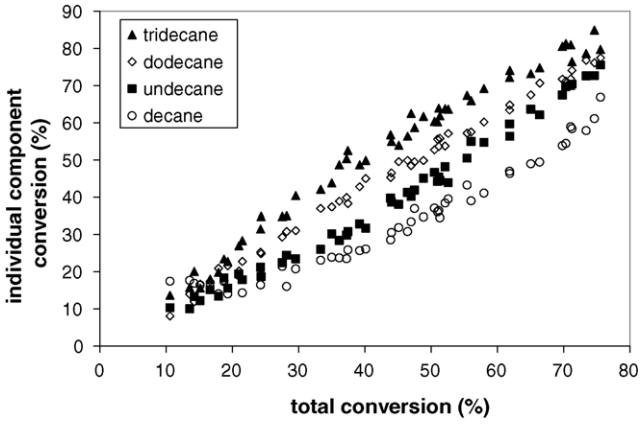

Fig. 4. Individual component conversion versus total parapur conversion in liquid phase hydrocracking at 513–533 K, 6–7.7 MPa and molar inlet hydrogen to hydrocarbon ratios between 3 and 8 [30].

Table 4
Comparison between individual component conversions in vapor and liquid phase parapur hydrocracking at 40 and 60% total parapur conversion [30]

	40%		60%	
	Vapor	Liquid	Vapor	Liquid
X_{C10}	19	28	36	46
X_{C11}	29	36	53	53
X_{C12}	43	40	65	60
X_{C13}	58	53	75	70

4. The gap between vapor and liquid phases

As evident from the discussion of the experimental results in Section 3 the hydrocracking mechanism constructed based on vapor phase experimental data can be used in the simulation of liquid phase experimental data. The main feature which needs to be addressed is the loss of the preferential physisorption of heavier hydrocarbons at liquid phase conditions compared to vapor phase conditions. In addition potential differences in acid strength of the catalyst's active sites induced by change in aggregation state are also accounted for.

The reference state used in the simulation of vapor as well as liquid phase hydrocracking is the ideal gas state. This allows a straightforward transition from vapor to liquid phase in the kinetic modelling and a clear comparison of the results obtained in both aggregation states. The phenomena that have to be accounted for when simulating liquid phase kinetics starting from vapor phase kinetics are:

1. Liquid phase fugacity to account for the deviation from the ideal gas state.
2. Physisorption excess: a destabilization of the sorbate molecules caused by compression and zeolite framework solvation.
3. Protonation excess: carbenium ion stabilization caused by the increased average acid strength of the catalyst due to framework solvation.

4.1. Fluid phase non-ideality

Using the ideal gas state as reference state, it is clear that the liquid phase behaves strongly non-ideal. This fluid phase non-ideality is accounted for by using fugacities rather than partial

pressures. Fugacities are the product of the fugacity coefficients and the partial pressures. The partial pressure can be further substituted as a function of the liquid phase concentration, liquid phase molar volume and the total pressure that can be easily measured or calculated at liquid phase conditions:

$$f_i = \phi_i p_i = \phi_i y_i p_t = \phi_i C_i V_m p_t \quad (10)$$

The fugacity coefficients are calculated as suggested by Reid et al. [22]. Peng Robinson's equation of state was used in the calculation of the compressibility factors. The higher the carbon number, the lower the fugacity coefficient. The fugacity coefficient is destabilizing the physisorption and is partly compensating the carbon number effect of the Henry coefficient: the fugacity coefficient decreases from 0.12 to 0.07 in the range of decane to tridecane at 506 K and 8 MPa.

4.2. Physisorption excess

The sorbate molecules exhibit liquid-like behavior in vapor phase as well as in liquid phase hydrocracking. The exact thermodynamic behavior of the sorbate depends on the aggregation state of the sorptive. On the one hand the high density of a liquid exerts a destabilizing compression effect, $\Delta G^{0,E}_{phys}$, on the sorbate molecules which is absent at low density, vapor phase conditions. On the other hand, the dense liquid phase is solvating the catalyst framework and, hence, physisorption within this zeolite framework will be affected. Drawing the analogy between the compression effect and the general fluid phase non-ideality a proportional relationship is put forward between the excess free enthalpy for physisorption and the fugacity coefficient:

$$\Delta G^{0,E}_{phys} \sim \ln \phi^L \quad (11)$$

The framework solvation is introduced into this expression as a framework dependent scaling factor, c^E:

$$\Delta G^{0,E}_{phys} = -c^E \ln \phi^L \quad (12)$$

The resulting values for the excess coefficients for physisorption range from 0.46 to 0.37 for decane to tridecane.

4.3. Protonation excess

The framework solvation by the liquid phase is not only inducing changes in physisorption behavior, but also in protonation behavior. The framework solvation leads to an increased strength of the acid sites. In agreement with earlier work 10 variations in acid strength are accounted for through the standard protonation enthalpy rather than the entropy. The parameter defined in this respect, i.e. the excess standard protonation enthalpy, is denoted as $\Delta H^{0,E}_{prot}$.

5. Estimation of excess properties

Single-event microkinetics (SEMK) for vapor phase hydrocracking have been applied using preliminary versions of the model [28,37], using SEMK at molecular level [10] and using relumped SEMK [9]. Standard protonation enthalpies leading to secondary and tertiary carbenium ions as well as the real single-event rate coefficients have been reported recently for octane hydrocracking on CBV-760, a Pt/H-USY [27]. These values have been used as reference values when applying SEMK to liquid phase hydrocracking data on MC-389. Two adjustable parameters are used in the simulation of the liquid phase data, i.e. c^E and $\Delta H^{0,E}_{prot}$ in the present work and constitute the model parameter vector b which is adjusted to minimize the sum of squares, cfr. Eq. (4).

The c^E scaling factor between the excess free enthalpy for physisorption and the liquid phase fugacity coefficient, vide Section 4.2, has been estimated from separate liquid phase physisorption measurements [36] and amounts to 1.55 ± 0.04 kJ mol^{-1}. The physisorption destabilization caused by the fluid non-ideality is enhanced by the physisorption excess due to this positive value for c^E. The combined destabilizing effect of fugacity coefficient and physisorption excess increases with carbon number and exactly compensates for the increasing Henry coefficients with carbon number.

Liquid phase parapur hydrocracking data [30] were used to estimate the protonation excess. The MC-389 catalyst used in [30] has similar acidic properties as the CBV-760 on which the reference kinetic parameters have been determined 27. As a result, the difference in standard protonation enthalpy obtained in this work compared to the reference value can be entirely attributed to the effect of the aggregation state on the strength of the acid sites. This excess standard protonation enthalpy, $\Delta H^{0,E}_{prot}$, amounts to -6 ± 0.4 kJ mol^{-1} leading to a standard protonation enthalpy of -65 kJ mol^{-1} for secondary carbenium ion formation and of -100 kJ mol^{-1} for tertiary carbenium ion formation. The higher acid strength leads to a higher carbenium ion stabilization at liquid phase conditions which is compensating for the physisorption destabilization.

The parity diagrams obtained during regression show a reasonable agreement between experimental and model-calculated values. Fig. 5 illustrates this agreement for the *n*-alkane lumps. The same quality of fit is obtained for the isomer and cracked product lumps per carbon number. Also the total

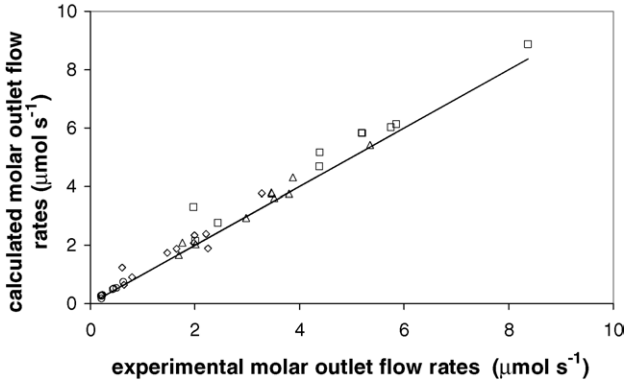

Fig. 5. Parity diagrams for the *n*-alkane lumps in liquid phase parapur hydrocracking: (○) *n*-decane, (Δ) *n*-undecane, (□) *n*-dodecane, (◇) *n*-tridecane. Operating conditions are mentioned in Table 1, the calculated results have been obtained using Eqs. (5) and (7) with the reference kinetic parameters from [27] and c^E and the protonation excess as estimated in this work.

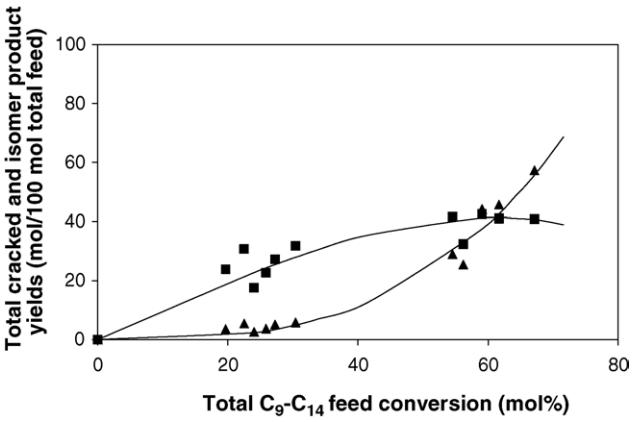

Fig. 6. Experimental (symbols) and simulated results (lines) for total isomer and cracked product conversion as a function of the total parapur conversion: (□) isomerization conversion, (Δ) cracking conversion. Operating conditions are mentioned in Table 1, the calculated results have been obtained using Eqs. (5) and (7) with the reference kinetic parameters from 27 and c^{E} and the protonation excess as estimated in this work.

parapur isomerization and cracked product conversion can be adequately described, vide Fig. 6. A good description of the liquid phase kinetics on USY is obtained by the model.

6. Conclusions

Physisorption effects play a key role in hydrocracking. The preferential conversion of heavier components in mixtures at vapor phase conditions is related to their higher Henry coefficients and their higher reactivity. The higher Henry coefficients of heavier hydrocarbons are compensated by their lower fugacity coefficients and physisorption excess coefficients at liquid phase conditions. As a result, the preferential conversion of heavier hydrocarbons at liquid phase conditions is solely due to their higher reactivity and, hence, is less pronounced.

The physisorption excess consists of a compression of the sorbate by the sorptive and a solvation of the framework, and leads to a destabilization of the sorbate molecules. The protonation excess accounts for the increase of the acid strength of the active sites at liquid phase conditions by the framework solvation and compensates for the physisorption destabilization.

A single-event microkinetic model accounting for liquid phase non-ideality, physisorption and protonation has been constructed. Apart from the independently determined reference kinetic parameters only two physically meaningful, adjustable parameters have been introduced:

1. c^{E}, a catalyst dependent scaling factor for the compression of sorbate molecules by the sorptive and
2. a difference in standard protonation enthalpy accounting for the increased acid strength of the zeolite by solvation.

A single-event microkinetic model using the reference kinetic parameters and these two physically meaningful adjustable parameters can adequately describe liquid phase parapur hydrocracking.

Acknowledgement

This research was carried out in the framework of the Interuniversity Attraction Poles Program funded by the Belgian Science Policy.

References

[1] D.M. Campbell, M.T. Klein, Appl. Catal. A-Gen. 160 (1997) 41.
[2] G.G. Martens, G.B. Marin, AIChE J. 47 (2001) 1607.
[3] D. Hudebine, J.J. Verstraete, Chem. Eng. Sci. 59 (2004) 4755.
[4] J.W. Thybaut, G.B. Marin, Chem. Eng. Technol. 26 (2003) 509.
[5] S. Katare, J.M. Caruthers, W.N. Delgass, V. Venkatasubramanian, Ind. Eng. Chem. Res. 43 (2004) 3484.
[6] S. Raimondeau, P. Aghalayam, A.B. Mhadeshwar, D.G. Vlachos, Ind. Eng. Chem. Res. 42 (2003) 1174.
[7] A. Schule, O. Shekhah, W. Ranke, R. Schlogl, G. Kolios, J. Catal. 231 (2005) 172.
[8] B. Debrabandere, G.F. Froment, Stud. Surf. Sci. Catal. 106 (1997) 379.
[9] G.G. Martens, G.B. Marin, J.A. Martens, P.A. Jacobs, G.V. Baron, J. Catal. 195 (2000) 253.
[10] J.W. Thybaut, G.B. Marin, G.V. Baron, P.A. Jacobs, J.A. Martens, J. Catal. 202 (2001) 324.
[11] J.A.M. Arroyo, G.G. Martens, G.F. Froment, G.B. Marin, P.A. Jacobs, J.A. Martens, Appl. Catal. A-Gen. 192 (2000) 9.
[12] J.A.M. Arroyo, J.W. Thybaut, G.B. Marin, P.A. Jacobs, J.A. Martens, G.V. Baron, J. Catal. 198 (2001) 29.
[13] P.B. Weisz, Adv. Catal. 13 (1962) 137.
[14] J. Weitkamp, H. Schulz, J. Catal. 29 (1973) 361.
[15] J. Weitkamp, K. Hedden, Chem. Ing. Tech. 47 (1975) 537.
[16] M. Steijns, G.F. Froment, Ind. Eng. Chem. Prod. Res. Dev. 20 (1981) 660.
[17] J.F. Denayer, G.V. Baron, W. Souverijns, J.A. Martens, P.A. Jacobs, Ind. Eng. Chem. Res. 36 (1997) 3242.
[18] R.D. Bezman, Stud. Surf. Sci. Catal. 68 (1991) 305.
[19] J.M. Berty, Chem. Eng. Prog. 70 (1974) 78.
[20] M. Steijns, G.F. Froment, P. Jacobs, J. Uytterhoeven, J. Weitkamp, Ind. Eng. Chem. Prod. Res. Dev. 20 (1981) 654.
[21] J.A. Mahoney, J. Catal. 32 (1974) 247.
[22] R.C. Reid, J.M. Prausnitz, B.E. Poling, The Properties of Gases and Liquids, McGraw Hill, 1987.
[23] H.H. Rosenbrock, Comput. J. 3 (1960) 175.
[24] D.W. Marquardt, Ind. Appl. Math. 11 (1963) 431.
[25] Netlib, http://www.netlib.org.
[26] E. Vynckier, G.F. Froment, Modeling of the kinetics of complex processes based upon elementary steps, in: G. Astarita, S.I. Sandler (Eds.), Kinetic and Thermodynamic Lumping of Multicomponent Mixtures, Elsevier, Amsterdam, 1991, p. 131.
[27] J.W. Thybaut, C.S. Laxmi Narasimhan, G.B. Marin, J.F.M. Denayer, G.V. Baron, P.A. Jacobs, J.A. Martens, Catal. Lett. 94 (2004) 81.
[28] G.D. Svoboda, E. Vynckier, B. Debrabandere, G.F. Froment, Ind. Eng. Chem. Res. 34 (1995) 3793.
[29] J.W. Thybaut, C.S. Laxmi Narasimhan, J.F. Denaeyer, G.V. Baron, P.A. Jacobs, J.A. Martens, G.B. Marin, Ind. Eng. Chem. Res. 44 (2005) 5159.
[30] B. Debrabandere, PhD Thesis, Ghent University, 1998.
[31] H.F. Schulz, J. Weitkamp, Ind. Eng. Chem. Res. Prod. Res. Dev. 11 (1972) 1.
[32] J. Weitkamp, Ind. Eng. Chem. Res. Prod. Res. Dev. 21 (1982) 550.
[33] J.A. Martens, P.A. Jacobs, J. Catal. 124 (1990) 357.
[34] J.F.M. Denayer, B.A. De Jonckheere, M. Hloch, G.B. Marin, G. Vanbutsele, J.A. Martens, G.V. Baron, J. Catal. 210 (2002) 445.
[35] J.F.M. Denayer, A.R. Ocakoglu, B.A. De Jonckheere, J.A. Martens, G.B. Marin, G.V. Baron, Int. J. Chem. React. Eng. 1 (A36) (2003) 1.
[36] J.F.M. Denayer, A. Bouyermaouen, G.V. Baron, Ind. Eng. Chem. Res. 37 (1998) 3691.
[37] M.A. Baltanas, K.K. Van Raemdonck, G.F. Froment, S.R. Mohedas, Ind. Eng. Chem. Res. 28 (1989) 899.